# Synthesis of Near-Infrared-Emitting, Water-Soluble CdTeSe/CdZnS Core/Shell Quantum Dots

Thomas Pons,*,† Nicolas Lequeux,‡ Benoit Mahler,† Siarhei Sasnouski,† Alexandra Fragola,† and Benoit Dubertret†

*Laboratoire Photons et Matière, CNRS UPRA0005, ESPCI, 10 rue Vauquelin, 75005 Paris, France, and Laboratoire de Physico-chimie des Polymères et Milieux Dispersés, CNRS UMR7615, ESPCI, 10 rue Vauquelin, 75005 Paris, France*

*Received October 6, 2008. Revised Manuscript Received February 4, 2009*

Applications of near-infrared (NIR) emitting CdTe-based QDs have been hampered by their sensitivity to oxidation. Here, we describe a synthetic method for the growth of CdTeSe/CdZnS core/shell QDs emitting in the NIR range (700−800 nm). We first synthesize high-quantum-yield zinc-blende CdTeSe cores with gradient composition and tunable emission up to 800 nm. The CdZnS shell growth is performed with cadmium and zinc carboxylate and trioctylphosphine sulfur precursors in trioctylamine solvent, and yields thick shell with controlled zinc blende crystalline structure. The presence of a high-band-gap, oxidation-resistant shell considerably improves the quantum yield and stability of these QDs when solubilized in saline buffers, making them promising fluorescence probes for NIR biological imaging.

The near infrared spectral range (700−900 nm) presents many advantages for in vivo fluorescence imaging. In particular, absorption of photons by biological tissues is much reduced in this spectral window compared to the visible range. This allows penetration of excitation and fluorescence photons deep into biological samples with reduced interaction and photodamage to the surrounding tissues, allowing fluorescence imaging depths on the order of centimeters. Another advantage of the low tissue absorption lies in the limited tissue autofluorescence, resulting in improved signal-to-noise ratio and sensitivity. The use of NIR organic fluorophores has opened the way to many valuable and diverse applications in small animal and human in vivo imaging, such as imaging of vascular structure in various organs, or the in vivo detection of protease activity and tumoral cells (see ref 1 and refs therein). However, conventional organic fluorophores present several drawbacks, including low fluorescence quantum yields and susceptibility to photobleaching.

Semiconductor quantum dots (QDs) have the potential to overcome these drawbacks and to significantly impact NIR fluorescence imaging applications. They present many advantages compared to organic fluorophores such as high photoluminescence (PL) quantum yield (QY), tunable emission wavelength, multiplexing capabilities, and high photoresistance.[2−4] These nanoscale materials have attracted much attention in the past decade and there have been many demonstrations of their use for biological imaging, ranging from single molecule tracking[5] to in vivo imaging[6,7] and immunological labeling.[8] The vast majority of these applications have used QDs based on II−VI materials, principally CdSe. The success of these materials can be attributed in part to the progress made in their synthesis and in particular in the growth of CdS, ZnS, or multilayer inorganic shells around CdSe cores to increase their QY and photoresistance by passivating their surface and protecting them against oxidation and from the effects of charges from the surrounding environment.[9−11] However, CdSe-based QDs can only reach typically 650−700 nm in emission, which is just below the optimal 700−900 nm NIR range for in vivo imaging. CdTe bandgap lies at 1.56 eV (corresponding to ∼795 nm wavelength), and 7 nm diameter CdTe QDs can reach ∼720 nm in emission. Recently, Rogach and co-workers described the aqueous synthesis of 8−10 nm CdTe-based QDs emitting at ∼800 nm.[12] Smaller NIR emitting QDs can be obtained with "type II" QDs, such as CdTe/CdSe core/shell systems

* Corresponding author. E-mail: thomas.pons@espci.fr.
† Laboratoire Photons et Matière.
‡ Laboratoire de Physico-chimie des Polymères et Milieux Dispersés.

(1) Frangioni, J. V. *Curr. Opin. Chem. Biol.* **2003**, *7*, 626–634.
(2) Efros, A. L.; Rosen, M. *Annu. Rev. Mater. Sci.* **2000**, *30*, 475–521.
(3) Medintz, I. L.; Uyeda, H. T.; Goldman, E. R.; Mattoussi, H. *Nat. Mater.* **2005**, *4*, 435–446.
(4) Michalet, X.; Pinaud, F. F.; Bentolila, L. A.; Tsay, J. M.; Doose, S.; Li, J. J.; Sundaresan, G.; Wu, A. M.; Gambhir, S. S.; Weiss, S. *Science* **2005**, *307*, 538–544.
(5) Dahan, M.; Levi, S.; Luccardini, C.; Rostaing, P.; Riveau, B.; Triller, A. *Science* **2003**, *302*, 442–445.
(6) Dubertret, B.; Skourides, P.; Norris, D. J.; Noireaux, V.; Brivanlou, A. H.; Libchaber, A. *Science* **2002**, *298*, 1759–1762.
(7) Kim, S.; Lim, Y. T.; Soltesz, E. G.; De Grand, A. M.; Lee, J.; Nakayama, A.; Parker, J. A.; Mihaljevic, T.; Laurence, R. G.; Dor, D. M.; Cohn, L. H.; Bawendi, M. G.; Frangioni, J. V. *Nat. Biotechnol.* **2004**, *22*, 93–97.
(8) Wu, X.; Liu, H.; Liu, J.; Haley, K. N.; Treadway, J. A.; Larson, J. P.; Ge, N.; Peale, F.; Bruchez, M. P. *Nat. Biotechnol.* **2003**, *21*, 41–46.
(9) Hines, M. A.; Guyot-Sionnest, P. *J. Phys. Chem.* **1996**, *100*, 468–471.
(10) Peng, X. G.; Schlamp, M. C.; Kadavanich, A. V.; Alivisatos, A. P. *J. Am. Chem. Soc.* **1997**, *119*, 7019–7029.
(11) Xie, R. G.; Kolb, U.; Li, J. X.; Basche, T.; Mews, A. *J. Am. Chem. Soc.* **2005**, *127*, 7480–7488.
(12) Rogach, A. L.; Franzl, T.; Klar, T. A.; Feldmann, J.; Gaponik, N.; Lesnyak, V.; Shavel, A.; Eychmuller, A.; Rakovich, Y. P.; Donegan, J. F. *J. Phys. Chem. C* **2007**, *111*, 14628–14637.

10.1021/cm8027127 CCC: $40.75 
Published on Web 03/16/2009

(up to 1 $\mu$m emission obtained with ~7−8 nm QDs),[13] or CdTeSe alloys.[14] Several proof-of-principle studies have demonstrated their use in vivo, in particular for vasculature and sentinel lymph node imaging.[7,15,16] Unfortunately, synthesis of these QDs has proved much more challenging and has not yet yielded QDs with PL QY and photoresistance comparable to their CdSe counterparts. CdTe and CdTe/CdSe QDs are prone to oxidation, which leads to low QY and fast photobleaching. The growth of protective inorganic shells around CdTe-based QDs is therefore of high importance. So far, there have been very few reports of higher bandgap shell growth around CdTe or CdTe/CdSe QDs. Jiang et al. showed that they were able to deposit only a very thin CdS shell (~1 monolayer) at the surface of a CdTeSe core.[17] Tsay et al.[18] presented a hybrid approach, necessitating the aqueous synthesis of CdTe and CdHgTe cores and their transfer to organic solvent, subsequent shell growth, and transfer back to water for biological application. Both syntheses made use of dimethylcadmium or diethylzinc and hexamethyldisilathiane precursors, which are highly toxic compounds and necessitate manipulation under an inert atmosphere. More recently, a report by Blackman et al. presented the synthesis of CdSe/CdTe/ZnSe multishell QDs emitting at 950−1000 nm using air stable precursors.[19,20] The presence of ZnSe shell was shown to significantly improve PL stability after water solubilization. Here we present a detailed synthesis that allows us to grow multilayer CdZnS shell around CdTeSe QDs using air stable carboxylate precursors. The resulting core−shell QDs can reach an 800 nm emission wavelength and exhibit improved photostability and quantum yields compared to CdTe core-only QDs when dispersed in water and saline buffers.

## Experimental Section

**Chemicals.** Trioctylphosphine (Cytop 380, TOP), cadmium oxide (99.99%, CdO), zinc oxide (99.99%, ZnO), octadecene (tech. 90%, ODE), selenium (99.99%), oleylamine (70%), oleic acid (tech., 90%), trioctylamine (90%), rhodamine 6G, and indocyanine green (ICG) were purchased from Sigma-Aldrich. Tellurium (99.999%) was purchased from Alfa Aesar. Tetradecylphosphonic acid (TDPA) was purchased from PCI Synthesis. DPPE-PEG2000-Me phospholipids were purchased from Novalyst. All chemicals were used directly without any further purification unless otherwise stated.

**Precursor Synthesis.** The $Cd(TDPA)_2$ precursor was prepared by mixing $n$ moles CdO with $2.05n$ moles TDPA in ODE (final Cd concentration 0.5M) and heating at 300 °C under argon. The resulting product is a white gel with a melting point around 200 °C. Cadmium oleate ($Cd(OA)_2$) and zinc oleate ($Zn(OA)_2$) 0.5 M stock solutions were prepared by heating CdO and ZnO powder in oleic acid at 180 and 240 °C, respectively, for 1 h, followed by degassing the resulting solutions at 80 °C under vacuum. TOPS, TOPSe, and TOPTe stock solutions were prepared by dissolution of S, Se, or Te powders in TOP at ambient temperature under inert atmosphere in a glovebox.

**CdTeSe Synthesis.** A typical CdTeSe synthesis is composed of two growth steps as described hereafter. First, 3.2 g of $Cd(TDPA)_2$ 0.5 M in ODE (~2 mmol Cd), 2 mL of TOP, and 2 mL of oleylamine were mixed with 5 mL of ODE in a three-neck flask. The preparation was degassed for 30 min under vacuum at 70−80 °C and then heated at 280 °C under argon. One-hundred microliters of 1 M TOPSe and 50 $\mu$L of 1 M TOPTe were mixed in 1 mL of TOP and swiftly injected. The solution was then kept at 230 °C for 10−20 min. Altenatively, CdTe (CdSe) nanocrystals could be synthesized by injection of 150 $\mu$L of 1 M TOPTe (TOPSe) instead. Additional growth is performed by dropwise injection of TOPSe 1 M at a 1.5 mL/h rate and stopped when the desired wavelength was obtained. The nanocrystals were precipitated twice in ethanol, and resuspended in 9 mL of hexane and 1 mL of TOP.

**CdS, CdZnS Shell Synthesis.** Typically, for a CdS shell synthesis, 2 mL of CdTeSe core solution were dissolved in 5 mL of trioctylamine, along with 0.5 mL of TOP and 0.6 mL of $Cd(OA)_2$ 0.5 M. The solution was degassed at 70−80 °C under a vacuum and heated at 230 °C. Six hundred microliters of TOPS 0.5 M solution were then injected dropwise in a few minutes, and the solution was kept at 230 °C for 30 min. A similar protocol was used to grow a CdZnS shell, except that 1.2 mL $Zn(OA)_2$ 0.5 M was added along with the $Cd(OA)_2$, and that the volume of injected TOPS 0.5 M was brought to 1 mL. The nanocrystals were precipitated in ethanol and resuspended in 10 mL of hexane.

**Characterization.** Photoluminescence and photoluminescence excitation spectra were acquired using a Fluoromax-3 fluorimeter (Jobin Yvon, Horiba). Photoluminescence quantum yields were measured using rhodamine 6G and indocyanine green (ICG) standards (95% in ethanol and 13% in DMSO, respectively). Optical densities (OD) of QD and dye standard solutions were measured using a Cary-5E UV−vis spectrophotometer (Varian) and the QYs were obtained following

$$QY_{QD} = QY_{dye} \frac{I_{QD}}{I_{dye}} \frac{OD_{dye}}{OD_{QD}} \frac{n_{QD}^2}{n_{dye}^2} \quad (1)$$

where $n_{QD,dye}$ is the refractive index and $l_{QD,dye}$ is the integrated fluorescence signal for the QD and dye solutions, respectively. Transmission electron microscopy (TEM) images were acquired on a JEOL 2010 field electron gun microscope. Elemental analysis was performed by energy-dispersive X-ray spectroscopy (EDS) on a Hitachi S-3600N scanning electron microscope. X-ray diffraction patterns were acquired using a Philips X'Pert diffractometer with a Cu K$\alpha$ source.

**Water Solubilization and Pinocytosis.** Solubilization of these nanocrystals was performed by encapsulation into amphiphilic phospholipid micelles. Typically, 200 $\mu$L of core/shell nanocrystals prepared as indicated above were washed with two cycles of precipitation in ethanol and resuspension in hexane, and finally resuspended in 100 $\mu$L of choloroform. The QDs were then mixed with 300 $\mu$L of DPPE-PEG2000-Me (dipalmitoyl phosphotidylethanolamine-polyethyelene glycol 2000-methyl ether) phospholipid solution at 20 mg/mL in chloroform and 1 mL of deionized water. The chloroform was evaporated by heating at 80 °C, yielding a limpid solution. These water-soluble QDs were then purified by ultracentrifugation following previously published protocols.[6,21]

The QDs were introduced in Hela P4 cells by osmotic lysis of pinosomes (OLP) using Influx Pinocytic Cell-Loading Reagent

(13) Kim, S.; Fisher, B.; Eisler, H. J.; Bawendi, M. *J. Am. Chem. Soc.* **2003**, *125*, 11466–11467.
(14) Bailey, R. E.; Nie, S. M. *J. Am. Chem. Soc.* **2003**, *125*, 7100–7106.
(15) Ballou, B.; Lagerholm, B. C.; Ernst, L. A.; Bruchez, M. P.; Waggoner, A. S. *Bioconjugate Chem.* **2004**, *15*, 79–86.
(16) Cai, W. B.; Shin, D. W.; Chen, K.; Gheysens, O.; Cao, Q. Z.; Wang, S. X.; Gambhir, S. S.; Chen, X. Y. *Nano Lett.* **2006**, *6*, 669–676.
(17) Jiang, W.; Singhal, A.; Zheng, J.; Wang, C.; Chan, W. C. W. *Chem. Mater.* **2006**, *18*, 4845–4854.
(18) Tsay, J. M.; Pflughoefft, M.; Bentolila, L. A.; Weiss, S. *J. Am. Chem. Soc.* **2004**, *126*, 1926–1927.
(19) Blackman, B.; Battaglia, D.; Peng, X. G. *Chem. Mater.* **2008**, *20*, 4847–4853.
(20) Blackman, B.; Battaglia, D. M.; Mishima, T. D.; Johnson, M. B.; Peng, X. G. *Chem. Mater.* **2007**, *19*, 3815–3821.

(Invitrogen). This technique was introduced by Okada and Rechsteiner and is based on the osmotic lysis of pinocytic vesicles.[22] The QDs were diluted in Hypertonic Loading Medium (HyperLM) at a final 0.1 $\mu$M QD concentration. All the solutions were warmed 20 min at 37 °C before use. Cultured cells were trypsinized and washed in DMEM. One mL of cell suspension with $1 \times 10^5$ cells/mL was centrifuged 1 min at 2000 rpm, the supernatant was removed and the cells were resuspended with 30 $\mu$L of QD-loaded HyperLM. After gentle agitation, the suspension was incubated for 4 min at 37 °C. This procedure leads to accumulation of QD-containing extracellular medium in vesicles. Osmotic lysis of pinocytic vesicles was performed by adding 2 mL of Hypotonic Lysis Medium (HypoLM) to the suspension and incubated 6 min at 37 °C. Finally, the cell suspension was centrifuged for 1 min at 2000 rpm and HypoLM was replaced by DMEM. Cells were washed 3 times in DMEM and were left for 10 min in the medium before imaging. A detailed manuscript on QD cellular labeling using pinocytosis is in preparation.[23]

QD-loaded cell fluorescence imaging was performed with an Olympus IX 71 microscope equipped with a Cascade 512B CCD camera (Roper Scientific). $512 \times 512$ pixels images were obtained using camera multiplication amplifier and readout speed of 5 MHz for increased image quality. A 550 nm low pass filter was used for excitation and a 590 nm long pass filter was used for detection (Chroma Technology).

## Results and Discussion

**CdTeSe QD Synthesis.** Synthesis of oxidation resistant II−VI nanocrystals emitting in the NIR requires starting from CdTe-based QD core and terminating the synthesis with a high bandgap shell such as ZnS or CdZnS. The lattice mismatch between CdTe and ZnS is particularly large (~17%) and is susceptible to induce strong local strain and generate nanocrystal dislocation.[24] To facilitate progressive adaptation of the lattice parameter, we chose to start from alloyed CdTeSe instead of pure CdTe cores. This choice is further motivated by the fact that CdTeSe alloy bandgaps may actually be smaller than that of pure CdTe, because of "optical bowing" effects, thus allowing reaching NIR emission wavelengths with smaller sized nanocrystals.[14]

CdTeSe nanocrystals were synthesized using Cd-tetradecylphosphonate (TDPA) and trioctylphospine (TOP)-Se and -Te precursors. Although many CdSe syntheses use cadmium carboxylate precursors, we found that these precursors yield very polydisperse CdTeSe QD populations and that nanocrystal growth is much better controlled using TDPA precursors. This may be attributed the very high reactivity of TOPTe compared to TOPSe with Cd carboxylates. Phosphonic acids are known to be stronger chelators of cadmium. They therefore provide lower reactivity precursors that allow better control on the nucleation and growth of CdTeSe nanocrystals. In a typical CdTeSe synthesis, a mixture of TOPSe and TOPTe precursors are swiftly injected at high temperature in an ODE solution containing TOP, oleylamine and $Cd(TDPA)_2$. After an initial growth period, further growth of the nanocrystals was performed by slow injection of additional TOPSe. Choice of cadmium precursors is not only important for control of CdTe and CdTeSe nucleation, but also for subsequent growth during reinjection of TOPSe. Indeed, when only $Cd(TDPA)_2$ is used, the QD population exhibit good size monodispersity and spheroidal shapes. However, when $Cd(TDPA)_2$ was used for nucleation and initial growth and ($Cd(OA)_2$) was reinjected along with TOPSe during the second growth step, the resulting CdTeSe QDs display similar PL and PLE properties, but exhibit tetrapod shapes, as shown in Figure 1. Because spheroidal shapes are more adapted to grow subsequent shells, $Cd(TDPA)_2$ was used as the only precursor for CdTeSe synthesis in this work. The resulting CdTeSe QD emission spectra gradually shift from ~550 to ~650 nm during initial growth after the first injection of TOPSe and TOPTe, with very high PL QYs, typically 60−80%. Reinjection of additional TOPSe precursors could then shift the QD PL emission to 800nm, as shown in Figure 1A, while preserving high QYs (50−60%). We note that the PL spectra somewhat broaden progressively during growth, as well as the PLE excitonic features. We attribute this to an increase in polydispersity in size and composition. In type II QDs, the strong PL red shift is accompanied by a decrease in the band edge exciton absorbance. In contrast, we note that the PLE of our large CdTeSe QDs shows more of a type I structure, with non vanishing PLE intensity at the band edge. This could be due to a CdTe-CdSe gradient composition instead of the well-separated core−shell structure in type II CdTe/CdSe QDs.

We examined the crystalline structure of these CdTeSe QDs by X-ray diffraction, as shown in Figure 2A. Diffraction peaks appear between those expected for CdTe and CdSe, consistent with a CdTeSe alloy composition. The diffraction pattern closely matches a zinc blende structure model. The second group of peaks ($2\theta \approx 40-50°$) show some intensity diffracted between the two main peaks, similar but broader and much weaker than in a pure wurtzite pattern, where the middle peak intensity is similar to the two other peaks (Figure 2A). We attribute this feature to the presence of stacking faults introducing small wurtzite domains in the predominantly zinc blende nanocrystals, consistently with what has been observed in recent reports.[25] This zinc blende structure is consistent with what has been previously reported with CdTe QDs synthesized with $Cd(TDPA)_2$ precursors. This is also consistent with the growth of CdTeSe/CdSe tetrapods with oleate precursor reinjection (Figure 1D), a shape that has been explained by the growth of wurtzite arms on a zinc blende core.[26]

Figure 2B shows Se:Te molar ratio in CdTeSe QDs obtained from energy dispersive X-ray spectroscopy (EDS), before and after injection of additional TOPSe. The CdTeSe QDs are initially Te-rich, even though the precursor solution is injected with a 2:1 Se:Te ratio, and becomes richer in Se as growth proceeds. This could be attributed to the higher

(21) Carion, O.; Mahler, B.; Pons, T.; Dubertret, B. *Nat. Protoc.* **2007**, *2*, 2383–2390.
(22) Okada, C. Y.; Rechsteiner, M. *Cell* **1982**, *29*, 33–41.
(23) Muro, E.; Sasnouski, S.; Fragola, A.; Dubertret, B. Manuscript in preparation.
(24) Ithurria, S.; Guyot-Sionnest, P.; Mahler, B.; Dubertret, B *Phys. Rev. Lett.* **2007**, 99.
(25) Smith, A. M.; Mohs, A. M.; Nie, S. *Nat. Nanotechnol.* **2009**, *4*, 56–63.
(26) Manna, L.; Milliron, D. J.; Meisel, A.; Scher, E. C.; Alivisatos, A. P. *Nat. Mater.* **2003**, *2*, 382–385.

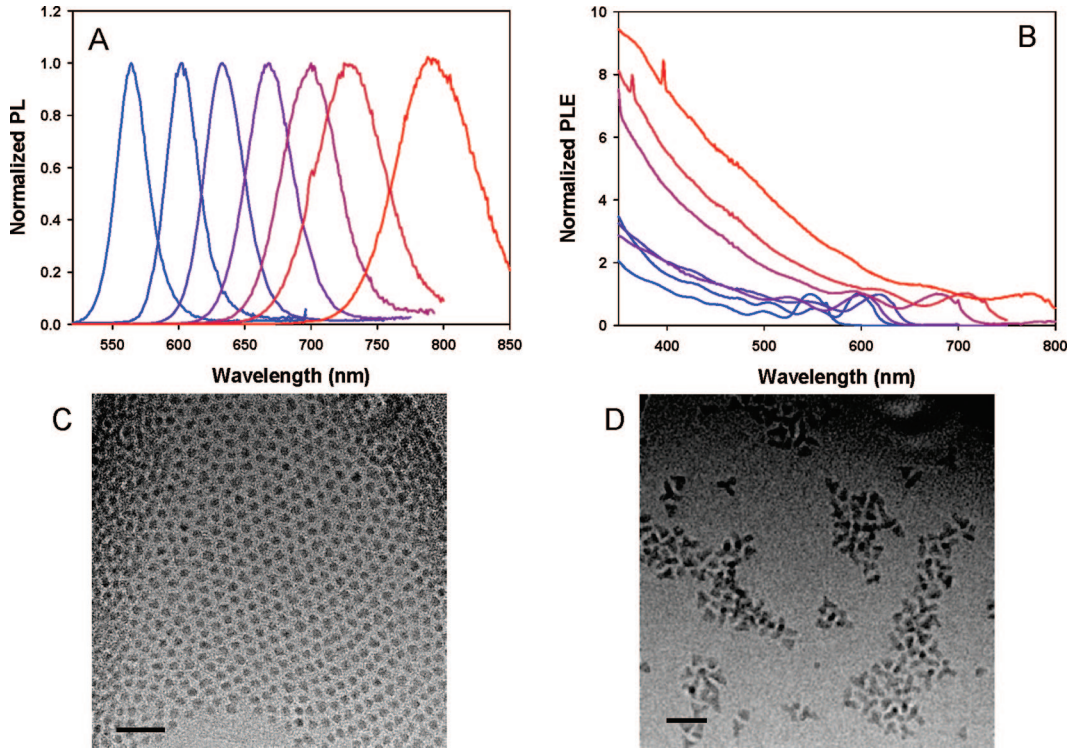


**Figure 1.** (A) Normalized PL spectra of different-sized CdTeSe QDs, corresponding to 30 s, 6 min, and 20 min after the first precursor injection, and 20, 30, 40, and 60 min after the start of the dropwise precursor reinjection. (B) PLE spectra of the same QDs, normalized at the first exciton peak. (C) TEM images from CdTeSe QDs synthesized using $Cd(TDPA)_2$ precursors. (D) TEM images from CdTeSe QDs synthesized using $Cd(TDPA)_2$ precursors in the first growth step and $Cd(OA)_2$ in the second growth step. Scale bars represent 20 nm.

reactivity of TOPTe compared to TOPSe. TOPTe is therefore expected to react first to form CdTe-rich nuclei. As the concentration of TOPTe in solution drops, further nanocrystal growth progressively introduces increasing amounts of CdSe.

Although CdTe QDs are very prone to oxidation, we observed that CdTeSe QDs were much more resistant to oxidation upon exposure to air (data not shown). On the other hand, although we could have expected the final CdTeSe QDs surface to be mainly composed of CdSe, we noted several significant differences between these CdTeSe QDs and CdSe QDs grown under similar conditions. For example, although CdSe QDs could be easily transferred to water with mercapto-undecanoic acid (MUA) following standard ligand exchange procedures, CdTeSe ligand exchange and transfer to water led to immediate aggregation. In addition, mixing CdTeSe QDs with a 0.1 M solution of sulfur diluted in ODE at room temperature led to immediate loss of PL, whereas it had no significant effect on CdSe QDs PL. This is consistent with a surface composed in part by Te atoms, and passivated with TOP ligands. This would prevent ligand exchange with thiolates such as MUA that bind to cationic surface sites. Furthermore, the PL loss in the presence of elemental sulfur could be attributed to detachment of TOP from QD Te surface sites to S atoms in solution. Finally, we observed that terminating the initial growth period by injecting excess $Cd(OA)_2$ without additional Se or Te precursors allows ligand exchange with thiolates and strongly reduces sensitivity to the presence of elemental sulfur in solution. However, a concomitant increase in polydispersity precluded the use of this final $Cd(OA)_2$ injection for the synthesis of high-quality core/shell QDs.

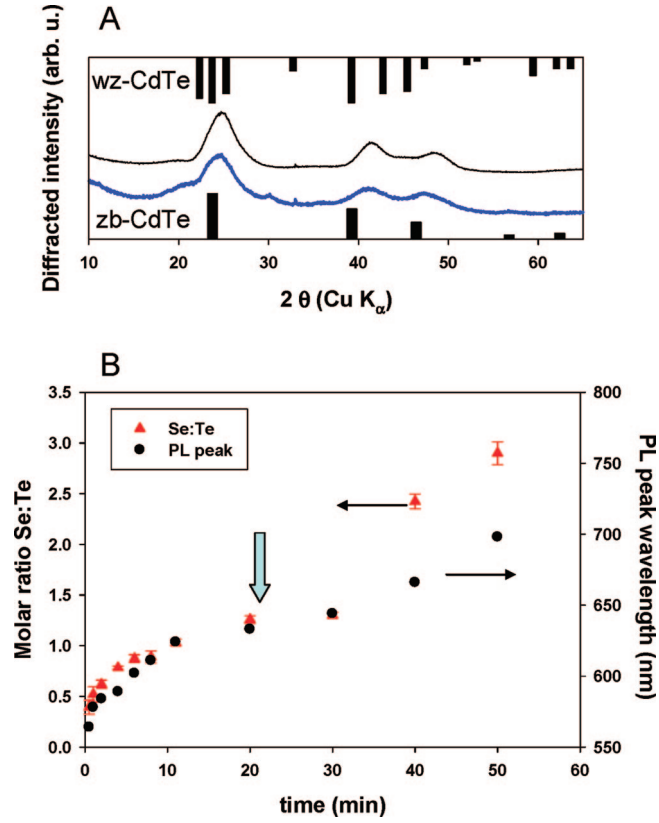


**Figure 2.** (A) X-ray diffraction pattern from CdTeSe QDs emitting at 700 nm (lower trace) and 800 nm (upper trace). Lower (upper) bars indicate peak positions and relative intensities for zinc blende (wurtzite) CdTe. (B) Evolution of Se:Te composition and PL peak wavelength as a function of time. The vertical arrow indicates the beginning of the second growth step.

**CdTeSe/CdZnS Synthesis.** The crystalline structure of these CdTeSe cores and the presence of Te atoms at or near their surface are strong limiting factors to obtain controlled spheroïdal core/shell QDs. We found that standard procedures to grow CdS or ZnS shells around CdSe QDs could not be simply transposed for growth around these CdTeSe QDs. In particular, we found that heating purified CdTeSe QDs in presence of trioctylphosphine oxide (TOPO), a standard ligand/coordinating solvent used for QD synthesis (see for example refs 9, 27 describing the growth of a ZnS or CdZnS shell over CdSe cores in TOPO), led to rapid and significant PL quenching. In addition, we found that synthetic methods using primary amines, such as successive ion layer adsorption and reaction (SILAR), favored growth of wurtzite arm structures, consistent with what has been shown with CdSe nanocrystals.[28] Because our CdTeSe cores were predominantly zinc blende, this led to the formation of tetrapod-shaped nanocrystals, similar to those observed when growing CdTeSe/CdSe with $Cd(OA)_2$ precursors (Figure 1D). Furthermore, primary amines were found to accelerate Oswald ripening of our purified CdTeSe QDs, which was much more pronounced than with CdSe QDs and led to rapid broadening of the size distribution and PL peak. Finally, the presence of TOP in the reaction solvent helped prevent QD aggregation during the reaction and limit their oxidation.

We therefore turned to a recently developed shell growth synthetic method using trioctylamine (TOA) and trioctylphosphine (TOP), with $Cd(OA)_2$, $Zn(OA)_2$ and TOPS precursors.[28,29] The use of trioctylamine improves the shell quality compared to ODE alone and allows conservation of zinc blende crystalline structure, as previously described with CdSe QDs.[28] The difference between primary and tertiary amines with respect to conservation of the core−shell crystalline structure may result from a reduced interaction of TOA with the QD surface compared to oleylamine, that could be due in part to steric hindrance from the three carbon chains and reduced affinity for II−VI atomic species. However, the CdTeSe cores were still subject to Oswald ripening, so that a balance needed to be found between slow, controlled shell growth and a fast but less-controlled growth that stabilizes the CdTeSe QDs before their Oswald ripening. In consequence, we chose a relatively low growth temperature, high precursor concentrations, and rapid injection. In a typical synthesis, shell growth occurred over a 30 min period, which is fast compared to other methods such as SILAR. Figure 3 show spectroscopic properties CdTeSe/CdS and CdTeSe/CdZnS core/shell QDs grown from CdTeSe cores emitting at 690nm. We observe a significant red shift of the QD bandgap during the growth, with the final core/shell QDs emitting at around 780−800 nm. The obtained core/shell PL QYs were typically 50%. PLE spectra show abrupt slope changes at around 500 nm, indicative of the presence of higher bandgap shells around the CdTeSe cores. We note again that the band edge exciton absorbance do not vanish, in contrast to type II QDs. This feature may be especially interesting for in vivo imaging where not only emission but also excitation wavelengths should be located in the NIR range. TEM images show that the core/shell QDs are slightly more polydisperse than the initial cores and are faceted, probably resulting from the absence of primary amines and the low growth temperature, which usually allow surface recomposition (Figure 4). High-resolution TEM imaging (Figure 4, right) shows that the most of the obtained core/shell QDs are monocrystalline and display a zinc blende

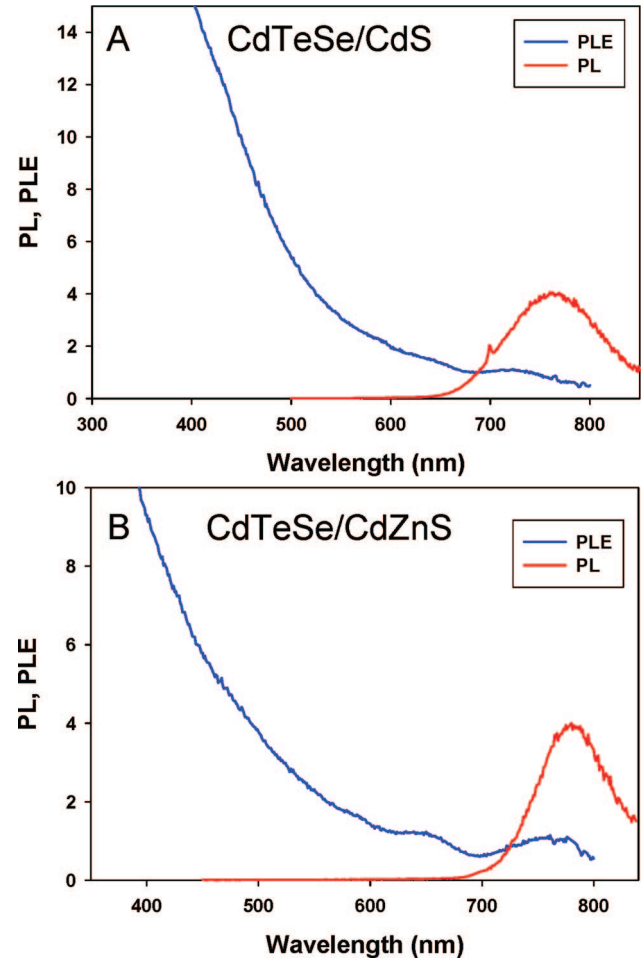


**Figure 3.** PL and EPL spectra from (A) CdTeSe/CdS and (B) CdTeSe/CdZnS core/shell QDs.

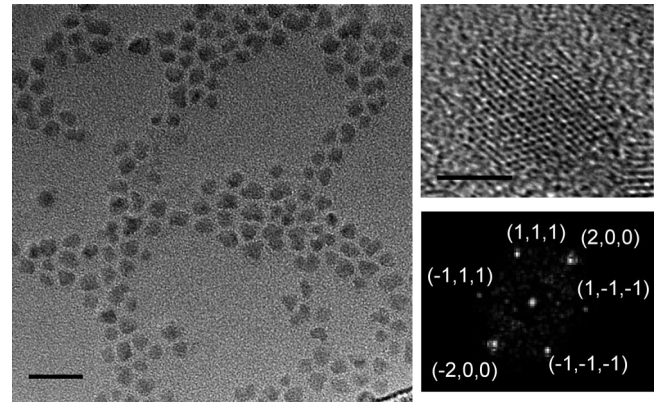


**Figure 4.** Left, TEM image of a representative sample of CdTeSe/CdZnS QDs (scale bar: 20 nm). Right, high-resolution TEM image of a CdTeSe/CdZnS QD (scale bar: 4 nm), along with the corresponding fast Fourier transform image. The diffracted pattern corresponds to the [0, 1, −1] zinc blende zone axis.

(27) Liu, W. H.; Choi, H. S.; Zimmer, J. P.; Tanaka, E.; Frangioni, J. V.; Bawendi, M. *J. Am. Chem. Soc.* **2007**, *129*, 14530–14531.
(28) Mahler, B.; Lequeux, N.; Dubertret, B. *Angew. Chem., Int. Ed.* Manuscript submitted.
(29) Jun, S.; Jang, E.; Lim, J. E. *Nanotechnology* **2006**, *17*, 3892–3896.

**Table 1. Elemental Composition of CdTeSe Initial Cores and Core/Shell QDs As Obtained from EDS, Normalized to Te Content (molar ratios compared to Te)[a]**

| | CdTeSe | CdTeSe/CdS | CdTeSe/CdZnS |
|---|---|---|---|
| S | | 9 ± 0. 3 | 5.2 ± 0.3 |
| Se | 2.1 ± 0.01 | 1.9 ± 0.3 | 2.1 ± 0.1 |
| Te | 1 | 1 | 1 |
| Cd | 5.1 ± 0.2 | 14 ± 0.4 | 7.3 ± 1 |
| Zn | - | | 2 ± 0.8 |

[a] ± values correspond to standard deviations from measurements on three different parts of the same sample.

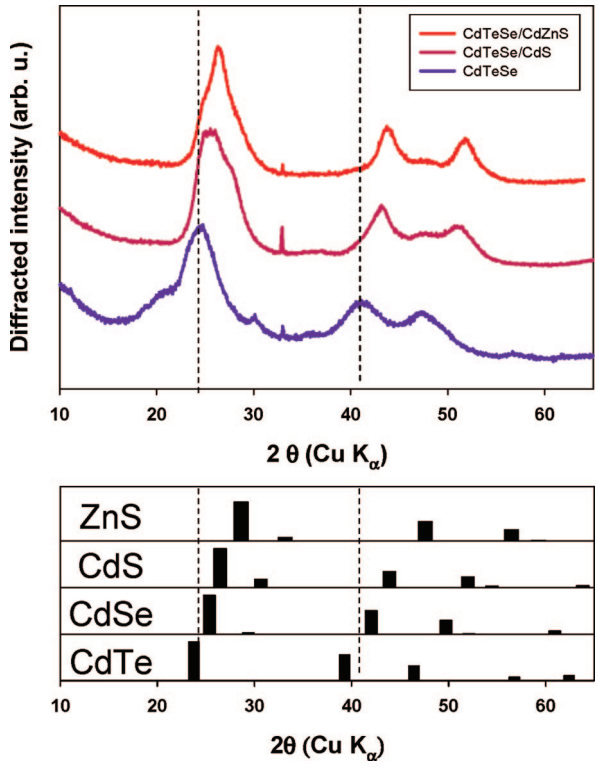


**Figure 5.** (Top) X-ray diffraction patterns from (bottom to top): CdTeSe, CdTeSe/CdS, and CdTeSe/CdZnS QDs. (Bottom) Theoretical X-ray diffraction patterns for bulk zinc blende CdTe, CdSe, CdS, and ZnS. Dashed lines are guidelines for the eyes.

structure, with some QDs displaying a few stacking faults. The core/shell structure is not distinguishable, as is often the case for QDs when the core and the shell have similar crystalline structures.

Elemental compositions of core and core/shell QDs were estimated by EDS and are summarized in Table 1. We observe that the Se:Te ratio is conserved during growth of the shell. In all samples, the measured cation composition is larger than the anion, which could be due to the presence of insoluble precursors (e.g., complexed by TDPA). The measured compositions are consistent with growth of CdS or CdZnS shells. The ratio of S from the shell versus (Se+Te) from the core indicates an approximate 3 monolayers shell thickness. This thickness is consistent with the increase in size observed in TEM pictures, from typically 3.5 nm for initial CdTeSe cores to 5.8 nm for final core/shell QDs. Despite the higher Zn precursor concentration (2:1 Zn:Cd ratio), the shell appears to be a CdZnS alloy with lower Zn content, because of the differences in precursor reactivity. Figure 5 shows X-ray diffraction patterns from CdTeSe before and after additional TOPSe injection, and

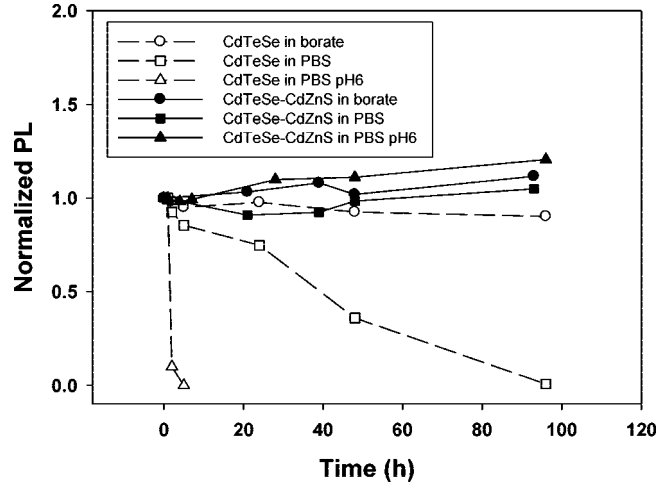


**Figure 6.** PL stability of phospholipid micelle encapsulated Cd-terminated CdTeSe and CdTeSe/CdZnS QDs in borate buffer and PBS at neutral and slightly acidic pHs.

from CdTeSe/CdS and CdTeSe/CdZnS core/shell QDs. These patterns closely resemble those of CdTeSe cores (Figure 2A), with the same predominant zinc blende structure. Again, we note the presence of a peak at around $2\theta \approx 47°$ between the (220) and (311) ZB peaks, but much smaller and broader, that is the signature of some stacking faults and small wurtzite domains.[25] This observation is consistent with the HRTEM images. We observe a progressive shift in the diffracted peaks positions consistent with the QD composition, as well as a narrowing of the peaks for core/shell QDs compared to core only QDs, confirming growth of a crystalline CdS and CdZnS shell on the nanocrystal cores.

**CdTeSe/CdZnS Water Solubilization and Cell Labeling.** CdTeSe cores and CdTeSe/CdZnS core/shell samples were prepared by encapsulation in polyethylene glycol (PEG) phospholipid micelles following previously described protocols.[6,21] The hydrophobic phospholipid carbon chains interdigitate with the carbon chains of the QD native ligands (mainly TOP or oleic acid), while the PEG moieties provide water solubilization and limit nonspecific adsorption of biomolecules. Encapsulation of as-prepared CdTeSe cores led to an immediate and complete PL quenching. This quenching was limited by terminating the CdTeSe core first growth step with an injection of excess $Cd(OA)_2$. We attribute this behavior to the low TOP-Te affinity at the surface of Te-terminated CdTeSe QDs. In contrast, Cd-terminated CdTeSe QDs are more stable because of the stronger interactions between oleic acid and Cd surface atoms. CdTeSe/CdZnS did not require any subsequent addition of cations for encapsulated QD preservation, and the resulting water-soluble QD PL QYs were typically 25−30% in water or immediately after dispersion in borate or PBS buffers.

We then compared the PL stability of core and core/shell QDs in borate (20 mM, pH ∼8) and PBS (pH ∼7.4 or pH ∼6.0) buffers. Borate is a relatively low salinity buffer, whereas the PBS salinity is closer to physiological conditions and its pH is adjusted to neutral and slightly acidic conditions. As shown in Figure 6, Cd-terminated CdTeSe PL was stable in borate buffer for several days. However, these core

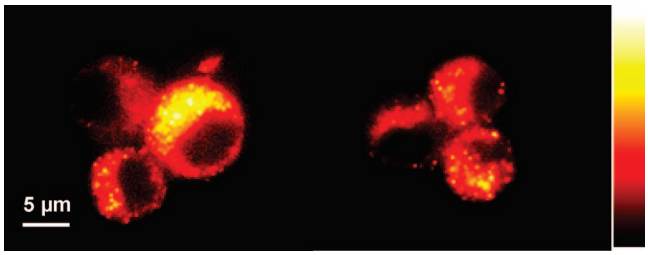


**Figure 7.** Fluorescence microscopy images from Hela $P\bar{4}$ cells labeled with CdTeSe/CdZnS QDs, represented with the pixel lookup table shown on the right.

QDs lost their PL in a few days in neutral PBS buffer, and in a few hours in PBS pH 6 buffer. In comparison, CdTeSe/CdZnS QDs showed no significant PL loss after one week, thanks to its thick oxidation-resistant CdZnS shell, even in slightly acidic conditions. These QDs could be stored several months in water at 4 °C with minimal PL loss (only ∼10% PL loss after 3 months) and without significant aggregation. These QDs were also stable in a wide salinity range, in up to 1 M NaCl, without loss of water solubility or PL.

Finally, we tested the CdTeSe/CdZnS QDs stability in a cellular environment. Hela $P\bar{4}$ cells were subjected to a pinocytosis protocol in presence of 100 nM PEG-phospholipid encapsulated QDs, washed 3 times with buffer to remove excess QDs, let incubated in DMEM buffer for 10 minutes at 37 °C before deposition on glass coverslips for fluorescence microscope imaging. As shown in Figure 7, cells showed bright and uniform fluorescence signals due to homogeneous QD loading into the cell cytoplasm.[23] QDs were noticeably absent from the nucleus. Diffusion of individual (blinking) intracellular QDs could be visualized for at least several minutes without significant photobleaching, as shown in the movie in the Supporting Information.

## Conclusion

We presented a new, simple synthetic method to grow CdTeSe/CdZnS core/shell QDs with emission in the near-infrared biological "transparency window". We found that careful choice of precursors was required to control the QD shape and crystallinity due to the initial zinc blende core structure and to allow the growth of thick (∼3 monolayers) uniform shells. Interestingly, these QDs exhibit a behavior slightly different from standard type II QDs, and can be efficiently excited in the NIR range. CdTeSe/CdZnS core/shell QDs can be easily transferred to water and exhibit high PL stability and relatively high PL QY (25−30%) in physiological buffers over extended period of times. Given the high versatility of phospholipid encapsulated QDs, we expect that these high-performance NIR fluorophores may find numerous applications in biological and biomedical imaging,[1,7] as well as stable inorganic emitters for optoelectronic applications.

**Acknowledgment.** We acknowledge the Région Ile-de-France and Agence Nationale pour la Recherche (ANR) for financial support. We are grateful to M. Hanafi for help with the EDS elemental analysis.

**Supporting Information Available:** Fluorescence microscopy movie of a CdTeSe/CdZnS labeled cell (AVI). This material is available free of charge via the Internet at http://pubs.acs.org.

CM8027127